Motion of a colloidal particle in an optical trap

Branimir Lukić,[1] Sylvia Jeney,[1,*] Željko Sviben,[1,†] Andrzej J. Kulik,[1] Ernst-Ludwig Florin,[2] and László Forró[1]
[1]*Institut de Physique de la Matière Complexe, Ecole Polytechnique Fédérale de Lausanne (EPFL), CH-1015 Lausanne, Switzerland*
[2]*Center for Nonlinear Dynamics, University of Texas, Austin, Texas 78712, USA*
(Received 14 March 2007; published 19 July 2007)

Thermal position fluctuations of a colloidal particle in an optical trap are measured with microsecond resolution using back-focal-plane interferometry. The mean-square displacement $\langle \Delta x^2(t) \rangle$ and power spectral density are in excellent agreement with the theory for a Brownian particle in a harmonic potential that accounts for hydrodynamic memory effects. The motion of a particle is dominated at short times by memory effects and at longer times by the potential. We identify the time below which the particle's motion is not influenced by the potential, and find it to be approximately $\tau_k/20$, where τ_k is the relaxation time of the restoring force of the potential. This allows us to exclude the existence of free diffusive motion, $\langle \Delta x^2(t) \rangle \propto t$, even for a sphere with a radius as small as 0.27 μm in a potential as weak as 1.5 μN/m. As the physics of Brownian motion can be used to calibrate an optical trap, we show that neglecting memory effects leads to an underestimation of more than 10% in the detector sensitivity and the trap stiffness for an experiment with a micrometer-sized particle and a sampling frequency above 200 kHz. Furthermore, these calibration errors increase in a nontrivial fashion with particle size, trap stiffness, and sampling frequency. Finally, we present a method to evaluate calibration errors caused by memory effects for typical optical trapping experiments.

DOI: 10.1103/PhysRevE.76.011112 PACS number(s): 05.40.Jc, 87.80.Cc, 82.70.Dd

I. INTRODUCTION

Optical traps [1] are used in soft-matter, biological, and statistical physics, e.g., in the characterization of the diffusion of colloidal particles [2,3], in rheology of complex fluids [4,5], in single-molecule studies of molecular motors [6,7], and in experimental tests of fluctuation theorems [8,9].

They are increasingly used solely for position detection, where the force on the particle exerted by the trap is minimized. Then, the trap ensures that the particle remains within the detector range, and it provides the light source for the detection. As a result, the motion of an essentially free particle can be observed at very short times, which can be used in the rheology of semiflexible polymers [4,5,10]. In recent years, effort has been devoted to increasing the temporal resolution of the position detection down to the microsecond range [11,12].

However, at such short time scales, the main feature of the particle's motion is the presence of hydrodynamic memory effects coming from the inertia of the fluid [13–16]. When the particle receives momentum from fluid molecules, it displaces the fluid in its immediate vicinity. The surrounding flow field is altered and acts back on the particle due to a non-negligible fluid inertia. The friction force then includes additional terms that depend on the particle's past motion, which leads to hydrodynamic memory effects. As their influence overlaps with the influence of the optical trapping potential [16], there is a need to know precisely the time evolution of the Brownian motion for a particle in an optical trap. At the same time, when the sphere's radius is known, the physics of Brownian motion in a harmonic potential can be used to calibrate the optical trap [17]. It has already been pointed out that neglecting hydrodynamic memory effects can lead to errors in the calibration of optical traps [18].

Here, we present a detailed study of the motion of a micrometer-sized colloidal particle confined by an optical trap. Since the force acting on the particle in an optical trap is harmonic [19], we fit to our experimental data the theory of Brownian motion of a particle in a harmonic potential, taking into account the hydrodynamic memory effects [18,20]. Clercx and Schram [20] gave an analytical solution of the Langevin equation for the mean-square displacement in the time domain, while Berg-Sørensen and Flyvbjerg [18] introduced the solution for the power spectral density in the frequency domain. We test both solutions down to a resolution of 2 μs. By comparing our data to the theory of a free Brownian particle that accounts for memory effects, we estimate the upper limit of the time region where the particle's motion is free from the influence of the potential. A similar analysis is performed in the frequency domain. Finally, we characterize the calibration error for the detector sensitivity and trap stiffness when memory effects are neglected, and we discuss their relevance for selected experiments in soft-matter, biological, and statistical physics.

II. EXPERIMENTAL METHOD

The optical trap is created by a neodymium-doped yttrium aluminum garnet (Nd:YAG) laser beam ($\lambda = 1064$ nm, IRLC-500-1064S, CrystaLaser, Reno, NV, USA), enlarged 20 times by a beam expander (Sill Optics, Wendelstein, Germany) and focused with a 63× water-immersion objective lens (numerical aperture 1.2, Olympus, Tokyo, Japan). An experimental setup similar to the one we used is described in detail in Ref. [12]. The spring constant depends linearly on the laser power and is varied by introducing different neutral density filters into the beam path. We use polystyrene spheres (radius $a = 0.27$, 0.33, 0.5, 0.74, 0.99, and 1.25 μm, Bangs Laboratories, Fishers, IN, USA) suspended in distilled water at a con-

*Corresponding author. sylvia.jeney@epfl.ch
†On leave from Department of Physics, University of Zagreb, Bijenička cesta 32, HR-10000 Zagreb, Croatia.

TABLE I. Overview of the characteristic times and frequencies for a Brownian particle in a harmonic potential. τ_p and τ_f are related to the Brownian particle through the properties of the particle with density ρ_p and radius a and of the fluid with density ρ_f and viscosity η. τ_k is connected to the property of the harmonic potential, its spring constant k, also referred to as the trap stiffness. The values are calculated for a polystyrene sphere ($a=0.5$ μm) in water ($\rho_p/\rho_f=1.05$, $\eta=0.001$ Pa s). The equivalent values in the frequency domain are ϕ_p, ϕ_f, and ϕ_k. ϕ_k corresponds to the corner frequency of the power spectrum.

Time constant (μs)	Frequency constant (MHz)	Determining factor
$\tau_p=m/(6\pi\eta a)=0.06$	$\phi_p=1/(2\pi\tau_p)=2.65$	Inertia of the particle
$\tau_f=a^2\rho_f/\eta=0.25$	$\phi_f=1/(2\pi\tau_f)=0.68$	Inertia of the surrounding displaced fluid
$\tau_k=6\pi\eta a/k=147$	$\phi_k=1/(2\pi\tau_k)=0.001$	Harmonic potential (optical trap) for $k_1=64$ μN/m

centration of 10^6 microspheres/ml. The suspension is loaded into a rectangular liquid cell (size $\approx 20\times 5$ mm^2 and thickness ≈ 100 μm). The interference pattern of the light scattered by the trapped particle and the unscattered laser light is projected onto an InGaAs quadrant photodiode in the back focal plane (G6849, Hamamatsu, Hamamatsu City, Japan). Changes in the interference pattern are directly converted into a position signal recorded in volts. For small displacements, the differential signals from the photodiode are proportional to the lateral displacement. The signal is amplified (Öffner Electronics, Plankstadt, Germany) and digitized to 12 bits (NI-6115, National Instruments, Austin, TX, USA).

The mean-square displacement $\langle \Delta x^2(t)\rangle$ and power spectral density $P(f)$ are calculated from the measured particle's trajectory. The detector sensitivity β that converts the acquired position signal from volts to nanometers and the spring constant k are obtained from fitting the theories presented in the next section to our data. In all the presented figures, $\langle \Delta x^2(t)\rangle$ and $P(f)$ are already divided by β.

III. THEORY

The motion of a Brownian particle is characterized by the Langevin equation

$$m\ddot{x} = F_{fr} + F_{th} + F_{ext}, \tag{1}$$

where m is the inertial mass of the particle, F_{fr} is the friction force, F_{th} is the force arising from random thermal fluctuations, and F_{ext} includes all external forces.

For a Brownian particle immersed in an incompressible fluid and confined by a harmonic potential,

$$F_{ext} = -kx \tag{2}$$

with k the spring constant.

The form of the friction force that accounts for the inertia of the fluid is given by [20]

$$F_{fr}(t) = -6\pi\eta a\dot{x} - \frac{2}{3}\pi a^3\rho_f\ddot{x} - 6a^2\sqrt{\pi\rho_f\eta} \times \int_0^t (t-t')^{-1/2}\ddot{x}(t')dt', \tag{3}$$

where a is the particle's radius, ρ_f the density, and η the viscosity of the fluid. The motion is then determined by three time constants (Table I). The first, $\tau_p=m/(6\pi\eta a)$, is defined by the inertia of the particle. The second, $\tau_f=a^2\rho_f/\eta$, is set by the inertia of the fluid displaced by the particle. The third time constant, $\tau_k=6\pi\eta a/k$, is determined by the spring constant of the harmonic potential and gives the time scale during which the particle experiences a drift back toward the potential minimum.

The solution of the Langevin equation for the mean-square displacement is then provided by Clercx and Schram [20] as

$$\langle \Delta x^2(t)\rangle = 2D\tau_k + \frac{2D}{\tau_p+\tau_f/9}\left(\frac{e^{z_1^2 t}\,\mathrm{erfc}(z_1\sqrt{t})}{z_1(z_1-z_2)(z_1-z_3)(z_1-z_4)} + \frac{e^{z_2^2 t}\,\mathrm{erfc}(z_2\sqrt{t})}{z_2(z_2-z_1)(z_2-z_3)(z_2-z_4)} + \frac{e^{z_3^2 t}\,\mathrm{erfc}(z_3\sqrt{t})}{z_3(z_3-z_1)(z_3-z_2)(z_3-z_4)} + \frac{e^{z_4^2 t}\,\mathrm{erfc}(z_4\sqrt{t})}{z_4(z_4-z_1)(z_4-z_2)(z_4-z_3)}\right), \tag{4}$$

where $D=k_BT/(6\pi\eta a)$ is the diffusion coefficient, and the coefficients z_1, z_2, z_3, and z_4 are the four roots of the equation

$$\left(\tau_p+\frac{1}{9}\tau_f\right)z^4 + \sqrt{\tau_f}z^3 + z^2 + \frac{1}{\tau_k} = 0.$$

For $t\to\infty$, Eq. (4) approaches the limit

$$\langle \Delta x^2(\infty)\rangle = \frac{2k_BT}{k}, \tag{5}$$

showing that motion is then dominated by the potential.

In the case of a free particle, i.e., $k=0$, the mean-square displacement is given by the relation [14]

$$\langle \Delta x^2(t)\rangle_{free} = 2Dt\left[1 - 2\sqrt{\frac{1}{\pi}\frac{\tau_f}{t}} + 4\frac{\tau_f}{t} - \frac{\tau_p}{t} + \frac{3}{t(5\tau_f-36\tau_p)^{1/2}}\left(\frac{1}{\alpha_+^3}e^{\alpha_+^2 t}\,\mathrm{erfc}(\alpha_+\sqrt{t}) - \frac{1}{\alpha_-^3}e^{\alpha_-^2 t}\,\mathrm{erfc}(\alpha_-\sqrt{t})\right)\right] \tag{6}$$

where $\alpha_\pm=(3/2)(3\pm(5-36\tau_p/\tau_f)^{1/2})/(\tau_f^{1/2}(1+9\tau_p/\tau_f))$.

If the inertial effects are neglected, i.e., $\tau_{p,f} \to 0$, the solution of the Langevin equation for particle in the harmonic potential simplifies to [21]

$$\langle \Delta x^2(t) \rangle_{no\ inertia} = 2\frac{k_B T}{k}(1 - e^{-t/\tau_k}). \tag{7}$$

In the long-time limit $t \to \infty$ of Eq. (6) or in the short-time limit $t \to 0$ of Eq. (7), free diffusive Brownian motion is recovered and follows the simple relation

$$\langle \Delta x^2(t) \rangle_{diff} = 2Dt. \tag{8}$$

For further discussion of the mean-square displacement in the experimental section, we introduce the dimensionless quantities

$$X(t) = \frac{\langle \Delta x^2(t) \rangle}{\langle \Delta x^2(t) \rangle_{diff}} \tag{9}$$

and

$$X_{free}(t) = \frac{\langle \Delta x^2(t) \rangle_{free}}{\langle \Delta x^2(t) \rangle_{diff}}. \tag{10}$$

Brownian motion is usually also characterized by the power spectral density $P(f)$ of the particle's fluctuations, which mirrors the mean-square displacement through the Fourier transform as

$$\langle \Delta x^2(t) \rangle = 2k_B T/k - 2\int_0^\infty e^{-2\pi i f t} P(f) df. \tag{11}$$

The solution of the Langevin equation for the power spectral density is given by Berg-Sørensen and Flyvbjerg as

$$P(f) = \frac{D}{\pi^2 f^2} \frac{1 + \sqrt{f/2\phi_f}}{(\phi_k/f - \sqrt{f/2\phi_f} - f/\phi_p - f/9\phi_f)^2 + (1 + \sqrt{f/2\phi_f})^2}, \tag{12}$$

where the characteristic frequencies ϕ_p, ϕ_f, and ϕ_k, with $\phi_{p,f,k} = 1/(2\pi\tau_{p,f,k})$, are listed in Table I. ϕ_k corresponds to the corner frequency of the power spectrum.

The same limiting behaviors as for the mean-square displacement can be directly derived for the power spectral density in Eq (12).

For $f \to 0$,

$$P(f) = \frac{4k_B T\gamma}{k}. \tag{13}$$

For $k = 0$,

$$P_{free}(f) = \frac{D}{\pi^2 f^2} \frac{1 + \sqrt{f/2\phi_f}}{(\sqrt{f/2\phi_f} + f/\phi_p + f/9\phi_f)^2 + (1 + \sqrt{f/2\phi_f})^2}. \tag{14}$$

For $\phi_{p,f} \to \infty$, Eq. (12) simplifies to

$$P_{no\ inertia}(f) = \frac{D}{\pi^2 f^2 [1 + (\phi_k/f)^2]}. \tag{15}$$

For $f \to 0$ in Eq. (14) or $f \to \infty$ in Eq. (15), diffusive motion is restored with

$$P_{diff}(f) = \frac{D}{\pi^2 f^2}. \tag{16}$$

Again, we define the dimensionless quantities

$$\tilde{X}(f) = \frac{P(f)}{P_{diff(f)}} \tag{17}$$

and $X_{free}(t)$

$$\tilde{X}_{free}(f) = \frac{P_{free}(f)}{P_{diff}(f)}, \tag{18}$$

corresponding to $X(t)$ and $X_{free}(t)$. Because $X(t)$ and $\tilde{X}(f)$ are mathematically equivalent, we discuss both interchangeably in the following.

IV. RESULTS AND DISCUSSION

By tracking the motion of an optically trapped sphere, we first verify experimentally Eqs. (4) and (12). After comparing our data to Eq. (6), we determine the time below which the particle's motion is free from the influence of the harmonic potential. Equivalently, we use Eq. (14) to determine the frequency above which the particle's motion is free from the influence of the harmonic potential. Then, we discuss the occurrence of free diffusive Brownian motion as given by Eq. (8) in our experimental system. Finally, we use our findings to estimate the calibration accuracy in experiments using optical traps.

A. Comparison of data and theory

$\langle \Delta x^2(t) \rangle$ and $P(f)$ for a particle ($a = 0.5\ \mu$m) trapped in a potential with a spring constant $k_1 = 64\ \mu$N/m are plotted as continuous lines in Figs. 1(a) and 1(b). The motion is recorded with an acquisition frequency of 5 MHz during 2 s. To avoid aliasing artifacts in the power spectral density of the signal, we analyze the signal as if it was sampled with an effective sampling rate of $f_S = 500$ kHz, corresponding to a time resolution of 2 μs (see Refs. [16,18] for more details). The upper limit for the power spectral density shown in the following figures is given by the Nyquist frequency, i.e., $f_S/2$. The dashed line corresponds to free diffusive Brownian motion [Eqs. (8) and (16), respectively]. For long times or low frequencies, the motion is dominated by the potential and approaches the limit of Eq. (5) for $\langle \Delta x^2(t) \rangle$ and Eq. (13) for $P(f)$. At short times or, equivalently, high frequencies, the continuous line deviates from the dashed line due to the inertia of the fluid, as described in detail elsewhere [16].

By dividing the continuous line by the dashed line in Figs. 1(a) and 1(b), we obtain $X(t)$ and $\tilde{X}(f)$, respectively. Both are plotted as dots for k_1, as diamonds for $k_2 = 17\ \mu$N/m, and as squares for $k_3 = 3\ \mu$N/m in Figs. 2(a) and 2(b). Changing k only varies τ_k, while τ_p and τ_f remain constant, as the particle's and the fluid's properties are fixed ($\tau_p = 0.06\ \mu$s, $\tau_f = 0.25\ \mu$s). The dotted lines in Figs. 2(a) and 2(b) represent Eqs. (9) and (17) calculated for each given potential. The continuous line in Figs. 2(a) and 2(b) represents the motion

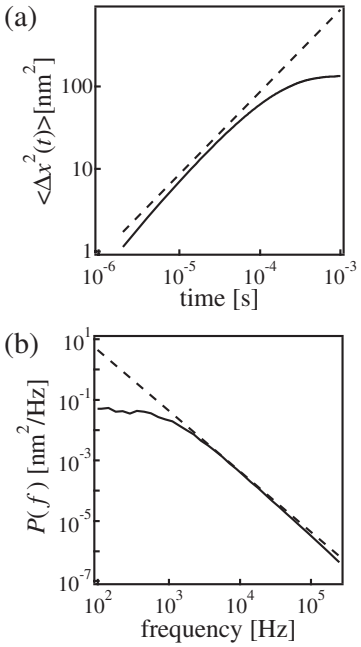

FIG. 1. Measured (a) $\langle \Delta x^2(t) \rangle$ and (b) $P(f)$ for a Brownian particle of radius 0.5 μm in a harmonic potential k_1=64 μN/m. Data for $P(f)$ are blocked in ten bins per decade. The dashed line indicates free diffusive Brownian motion [Eqs. (8) and (16)]. Data are calibrated using the value for detector sensitivity from Table II.

of the free particle, according to Eqs. (10) and (18), respectively.

At $t=\tau_k$, Eq. (9) gives the approximate value

$$X(t=\tau_k) \approx 1 - 1/e \cong 0.625, \tag{19}$$

which is indicated by the dashed horizontal line in Fig. 2(a). Thus, the intersection of the dotted line with the dashed line corresponds to τ_k. Similarly, Eq. (17) gives

$$\tilde{X}(f=\phi_k) \approx 0.5, \tag{20}$$

and also ϕ_k can be directly read from Fig. 2(b).

By taking ten data points per decade of time, Eq. (4) fits the measured $\langle \Delta x^2(t) \rangle$ with an accuracy better than 6% in the time interval between 100 μs and 1 ms, and even with an accuracy of 2% in the interval between 2 and 100 μs. For the power spectral density, values are distributed exponentially and therefore blocked in five bins per decade for fitting by the least-squares method [18]. Equation (12) fits the blocked values in the range between 100 Hz and 10 kHz with an accuracy better than 6%, and even 2% between 10 and 250 kHz. For fitting $\langle \Delta x^2(t) \rangle$ and $P(f)$, only two fitting parameters are needed, the detector sensitivity β and the spring constant k, which are given in Table II [22]. They agree with each other, as expected. The relative difference for all values of β is less than 0.5%. For k_1 and k_2 differences are smaller than 4%, whereas for k_3, they are larger than 10%, as τ_k is outside the fitting range. A better precision for such soft trapping potentials can be obtained by extending this range by using longer acquisition times, as discussed in the next section.

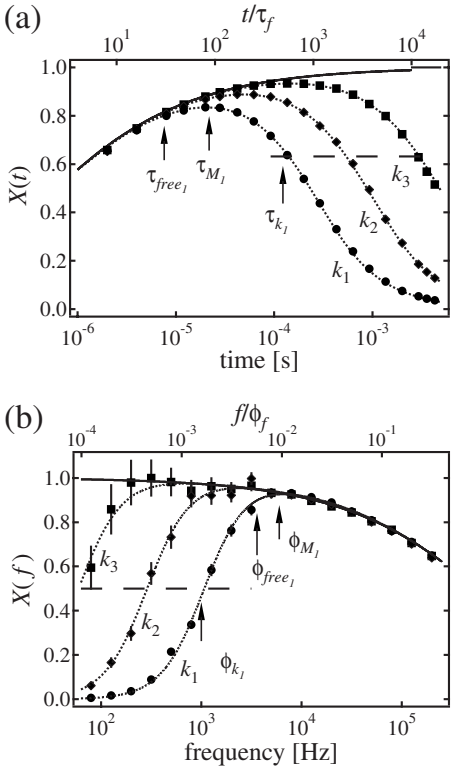

FIG. 2. (a) Equation (9) (dotted lines) fitted to the measured $X(t)$ for a polystyrene sphere (a=0.5 μm) in the optical trap at various spring constants (k_1=64 μN/m ●, k_2=17 μN/m ◆, k_3=3 μN/m ■). (Only six data points per decade are shown for the sake of clarity.) (b) Measured $\tilde{X}(f)$ for the same time traces. Data are blocked in five bins per decade, and error bars indicate the standard deviation. Equation (17) (dotted lines) is fitted to the data. $X_{free}(t)$ [Eq. (10)] and $\tilde{X}_{free}(f)$ [Eq. (18)] for a free particle are indicated by a continuous line.

Having demonstrated agreement between theory and data, we focus on the point where the dotted line starts to deviate from the continuous line. This sets the time below which the motion is free from the influence of the potential. Therefore, we define the time τ_M when $X(t)$ reaches its maximum, and the time τ_{free} starting from which $X(t)$ deviates from $X_{free}(t)$ by at least 2%. Both times are specified as a convenient estimate of an upper limit of the range during which the particle's motion can be considered as effectively free.

Together with τ_k, τ_M, and τ_{free} are indicated by arrows in Fig. 2(a) for the particle in potential k_1. For each potential represented in Fig. 2(a), there is a time range for which data follow $X_{free}(t)$ (continuous line), indicating that the motion is then independent of k. Equivalently, we define the frequency ϕ_M when $\tilde{X}(f)$ reaches its maximum, and ϕ_{free} as the frequency at which $\tilde{X}(f)$ deviates from $\tilde{X}_{free}(f)$ by 2%, indicated by arrows in Fig. 2(b). As τ_M and τ_{free} are not defined as characteristic times, we do not expect them to follow the relation $\tau_{M,free}=1/(2\pi\phi_{M,free})$ as it is the case for times in Table I.

In the next section, we establish their dependence on the particle size and the spring constant, and discuss their use to estimate the upper limit of the time range during which the particle's motion can be considered as free.

TABLE II. Parameters β and k as obtained from fitting Eq. (4) to $\langle \Delta x^2(t) \rangle$ and Eq. (12) to $P(f)$. τ_k and frequency ϕ_k are calculated from k and compared to τ_f and ϕ_f.

	Clercx and Schram, [20] Eq. (4)			Berg-Sørensen and Flyvbjerg, [18] Eq. (12)		
Trap	β (V/nm)	k (μN/m)	τ_k	β (V/nm)	k (μN/m)	ϕ_k
k_1	0.2350	64.2	0.147 ms$=0.6\times10^3\tau_f$	0.2362(5)	66.6±1.3	1130 Hz$=17.7\times10^{-4}\phi_f$
k_2	0.1090	17.0	0.554 ms$=2.2\times10^3\tau_f$	0.1095(4)	17.3±0.5	292 Hz$=4.5\times10^{-4}\phi_f$
k_3	0.0468	3.1	3 ms$=12.2\times10^3\tau_f$	0.0470(2)	3.6±0.2	60 Hz$=0.9\times10^{-4}\phi_f$

B. Dependence of τ_M and τ_{free} on a and k

In order to study the dependence of τ_M on a and k, we record the motion of different sphere sizes (a=0.27, 0.33, 0.5, 0.74, 0.99, and 1.25 μm) confined by potentials with a spring constant ranging from 1 to 100 μN/m. For stronger traps ($\tau_k<1$ ms), data are recorded at 500 kHz for 10 s and calibrated in the range between 2 μs and 1 ms. For softer traps ($\tau_k>1$ ms), data are recorded at 200 kHz for 50 s and calibrated between 5 μs and 10 ms. In Fig. 3(a), τ_M is plotted versus τ_k. The dashed lines show the theoretical predictions obtained numerically [23] for τ_M for different sphere radii. In this log-log representation, τ_M increases linearly with τ_k, indicating a power-law dependence, and data are shifted upward for larger a.

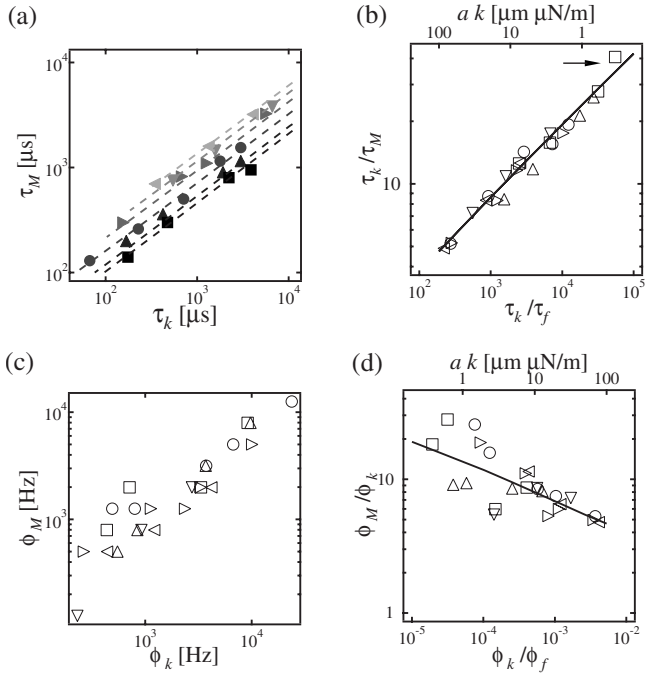

FIG. 3. (a) Time τ_M at which $X(t)$ reaches its maximum versus τ_k (a=0.27 μm, □; 0.33 μm, △; 0.50 μm, ○; 0.74 μm, ▷; 0.99 μm, ▽; 1.25 μm, ◁) and theoretical prediction from Eq. (9) for each particle size (dashed lines). (Data and theory are given in grayscale to show the increase of τ_M with increasing a.) (b) τ_k/τ_M versus τ_k/τ_f (bottom axis) and versus ak (top axis). The continuous line shows the theoretical prediction derived from Eq. (9). (c) Frequency ϕ_M at which $\tilde{X}(f)$ reaches its maximum versus ϕ_k and (d) ϕ_M/ϕ_k versus ϕ_k/ϕ_f (bottom axis) and versus ak (top axis). The continuous line in (d) shows theoretical prediction from Eq. (17).

To identify the power law, data are plotted as τ_k/τ_M versus τ_k/τ_f in Fig. 3(b) and analyzed in the range between 10^2 and $10^5\tau_k/\tau_f$. Using the first derivative of Eq. (9) [23], we find

$$\tau_k/\tau_M \propto (\tau_k/\tau_f)^\alpha \quad \text{with } \alpha = 1/3 \tag{21}$$

shown in Fig. 3(b) as a continuous line. This is equivalent to

$$\tau_M \propto a^{\alpha+1}k^{\alpha-1} = a^{4/3}k^{-2/3}. \tag{22}$$

Fitting the power law to our data using the least-squares method gives α=0.38±0.02, in agreement with the predicted α. Thus, the ratio τ_k/τ_M remains constant as long as $\tau_k/\tau_f \propto (ak)^{-1}$ is not changed [ak is given on the top axis in Fig. 3(b)].

The same procedure is applied for $\tilde{X}(f)$ to identify the dependence of ϕ_M on a and k. ϕ_M is defined as the average frequency of the bin for which $\tilde{X}(\phi_M)$ is maximal. Results are plotted in Fig. 3(c), and ϕ_M/ϕ_k versus ϕ_k/ϕ_f in Fig. 3(d). The continuous line in Fig. 3(d) is the theoretical prediction obtained numerically [23]. As for $X(t)$, the first derivative of Eq. (17) predicts a power law. However, estimating ϕ_M from a blocked data set is imprecise, as it can only be estimated with an error corresponding to the bin width. Since we have only five bins per decade, the error in estimation is large.

Next, we study the dependence of τ_{free} on a and k using the same data sets as described in Fig. 3. τ_{free} is plotted in Fig. 4(a) as a function of τ_k, and τ_{free}/τ_k versus τ_k/τ_f (bottom axis) or product ak (top axis) in Fig. 4(b). By calculating the 2% deviation of Eq. (9) from Eq. (10), we obtain $\tau_k/\tau_{free} \approx 16$ for $\tau_k/\tau_f \approx 10^2$ and $\tau_k/\tau_{free} \approx 25$ for $\tau_k/\tau_f \approx 10^5$ [Fig. 4(b), solid line]. The average value of our data in the measured range is τ_k/τ_{free}=20±4, leading to the approximation

$$\tau_{free} \approx \tau_k/20. \tag{23}$$

For the same data set we plot ϕ_{free} versus ϕ_k in Fig. 4(c), and ϕ_{free}/ϕ_k versus ϕ_k/ϕ_f in Fig. 4(d). By calculating the 2% deviation of Eq. (17) from Eq. (18), we obtain $\phi_k/\phi_{free} \approx 6$ for $\phi_k/\phi_f \approx 10^{-5}$ and $\phi_k/\phi_{free} \approx 4$ for $\phi_k/\phi_f \approx 10^{-2}$ [Fig. 4(d), solid line]. The average value of our data in the measured range is ϕ_{free}/ϕ_k=5±2, leading to the approximation

$$\phi_{free} \approx 5\phi_k. \tag{24}$$

Equations (23) and (24) give a fast estimation of the influence of the harmonic potential on the particle's motion. Their use will be shown in the next section.

Both times τ_M and τ_{free} give an upper limit for the time range during which the particle can be considered as free

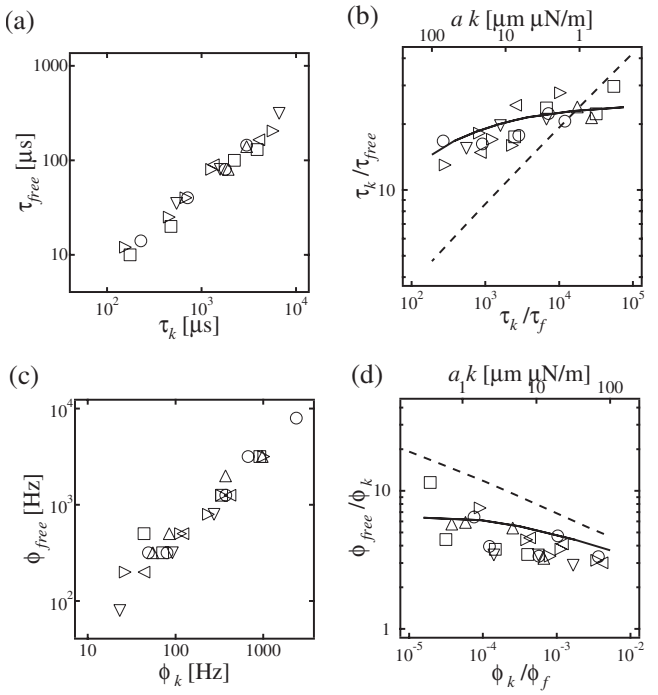

FIG. 4. (a) τ_{free} plotted versus τ_k for polystyrene spheres of different radii ($a=0.27$ μm, □; 0.33 μm, △; 0.50 μm, ○; 0.74 μm, ▷; 0.99 μm, ▽; 1.25 μm, ◁). (b) τ_k/τ_{free} versus τ_k/τ_f (bottom axis) and versus ak (top axis) The continuous line shows theoretical prediction (see text). Prediction for τ_k/τ_M from Eq. (21) is given by dashed line. (c) ϕ_{free} plotted versus ϕ_k. (d) ϕ_{free}/ϕ_k versus ϕ_k/ϕ_f (bottom axis) and ak (top axis). The continuous line in (d) shows theoretical prediction (see text). Prediction for ϕ_M/ϕ_k from Fig. 3(d) is given by dashed line.

from the influence of the trapping potential. However, the variation of τ_k/τ_{free} [Fig. 4(b), continuous line] with τ_k/τ_f is less rapid than the variation of τ_k/τ_M, which changes by an order of magnitude in the investigated range [Fig. 4(b), dashed line]. Moreover, we find that τ_{free} is more convenient to calculate than τ_M, as it is given by the simple relation in Eq. (23), which is independent of τ_f. Furthermore, $X(\tau_{free})/X_{free}(\tau_{free})=0.98$ does not depend on τ_k/τ_f, unlike $X(\tau_M)/X_{free}(\tau_M)$, which changes from 0.92 for $10^2\tau_k/\tau_f$ to 0.98 for $10^4\tau_k/\tau_f$.

C. Absence of free diffusive Brownian motion in an optical trap

Having identified a simple method to calculate τ_{free}, we can address the question of the nature of the particle's motion in the optical trap at times shorter than τ_k. To discuss this issue, we measured the trajectory of a small particle ($a=0.27$ μm) as the hydrodynamic memory effects decrease with decreasing particle size, and in a soft potential ($k=1.5$ μN/m), as the time region where the particle's motion is free from the influence of the trap lasts longer for high τ_k. This measurement corresponds to the data point highlighted by an arrow in Fig. 3(b). It is compared to Eq. (9) (dotted line) and Eq. (10) (continuous line) in Fig. 5(a). $X(t)$ reaches a maximum of ≈0.96. Equivalently, $\tilde{X}(f)$ is compared to Eq. (17) (dotted line) and Eq. (18) (continuous line) in Fig. 5(b). To obtain sufficient accuracy for $\tilde{X}(f)$, we average over five power spectra, each acquired with 200 kHz during 50 s, and block in ten bins per decade. In the range between 100 Hz and 10 kHz, the data agree with the theory within 2%. $\tilde{X}(f)$ has a maximum of ≈0.99.

Free diffusive Brownian motion is given by Eq. (8), implying $X(t)=1$ and equivalently $\tilde{X}(f)=1$. For the free particle $X_{free}(t)=1$ would occur within 2% error after approximately 200 μs$=3\times10^3\tau_f$ [Fig. 5(a), arrow]. Thus, to observe free diffusive Brownian motion, the optical trap would have to be so weak that $\tau_{free}>3\times10^3\tau_f$ is satisfied, or equivalently $\tau_k \geqslant 5\times10^4\tau_f$ according to Eq. (23). For the particle size and spring constant studied above, $\tau_k\approx4.8\times10^4\tau_f$. To observe free diffusive Brownian motion for at least one decade in time, the condition is $\tau_k/\tau_f\approx7\times10^7$. For the particle with $a=0.27$, this corresponds to a spring constant $k<10^{-3}$ μN/m. Such a low spring constant does not allow us to trap and observe the particle. Hence, in experiments using optical traps, the motion of a particle is influenced by either memory effects or the harmonic potential.

D. Calibration of an optical trap

In principle, the optical trap should be calibrated using a theory that accounts for hydrodynamic effects [18], i.e., using Eq. (12) instead of Eq. (15) for fitting the power spectrum. However, in some cases these effects can be neglected.

To quantify the error in calibration arising from neglecting inertial effects, we analyze the motion of different spheres ($a=0.27$, 0.33, 0.5, 0.74, 0.99, and 1.25 μm) confined by potentials with comparable values of k (2.3, 2.2, 3.6, 1.8, 2.0, and 4.9 μN/m, respectively). First, we fit Eq. (12) to the power spectrum in the range between 1 Hz and the upper limit f_{max}, and obtain β and k. Then we fit Eq. (15) to the power spectrum and obtain β' and k'. $\varepsilon_\beta=1-\beta'/\beta$ and $\varepsilon_k=1-k'/k$ is the calibration error for β and k, respectively, if memory effects are neglected. The dependence of ε_β and ε_k on a is plotted in Figs. 6(a) and 6(b), respectively for $f_{max}=10$ or 100 kHz. A positive error corresponds to an underestimation of the fitting parameter by using Eq. (15) rather than Eq. (12).

We observe that ε_β and ε_k increase with a, as well as with f_{max}. Fitting according to Eq. (15) is justified only when data are acquired with a sampling frequency such that $f_S\equiv f_{Nyq}<10^{-4}\phi_f$. Here, f_{max} corresponds to f_{Nyq}. As $\phi_f\propto 1/a^2$ (Table I), such fitting works better for smaller particles and smaller sampling frequencies, and hence calibration errors are smaller.

If we take f_{max} to correspond to the Nyquist frequency $f_S/2$, we can make a general statement using Fig. 6: errors are larger than 10% when data are acquired with an acquisition frequency larger than 200 kHz for particles with radii larger than 0.5 μm.

However, in Fig. 6, the calibration errors are represented only for very soft traps. But, as k cannot be changed continuously due to experimental limitations, we use the theory to estimate the dependence of ε_β and ε_k on k. We first calculate

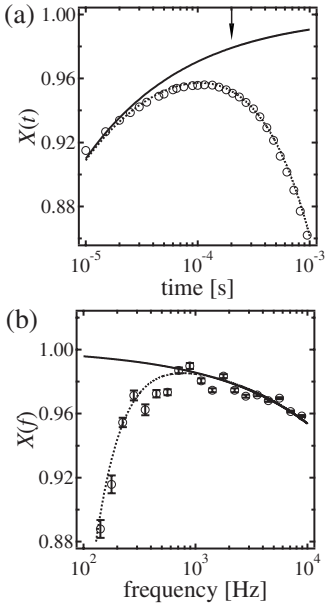

FIG. 5. (a) $X(t)$ for the sphere with $a=0.27\ \mu$m and $k=1.5\ \mu$N/m, compared to the theory in Eq. (9) (dotted line). Theory for the free particle $X_{free}(t)$ is given by the continuous line [Eq. (10)], and time when $X_{free}(t)$ reaches the value of 0.98 is indicated by an arrow. (b) $\tilde{X}(f)$ for the same sphere compared to the theory in Eq. (17) (dotted line). The free particle case is given by a continuous line [Eq. (18)].

the theoretical power spectrum with Eq. (12) for various combinations of a and k, block it in ten bins per decade, and then fit it as above to obtain ε_β and ε_k. The fitting range is varied between 1 Hz and f_{max}. Figure 7 shows a contour plot

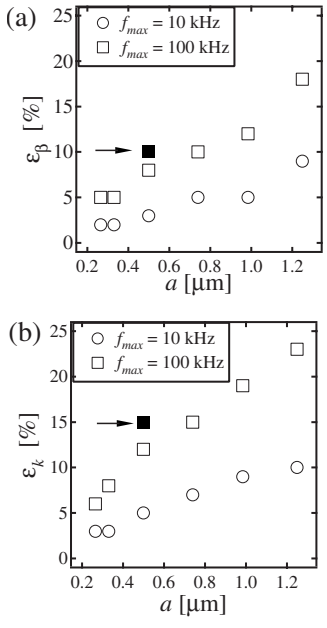

FIG. 6. Underestimation error (a) ε_β for the detector sensitivity β and (b) ε_k for the spring constant k, if inertial effects are neglected. Theories are fitted to the power spectrum in the fitting range between 1 Hz and $f_{max}=10$ kHz (○) and 100 kHz (□). The error for the particle from Fig. 2 is highlighted as a full square.

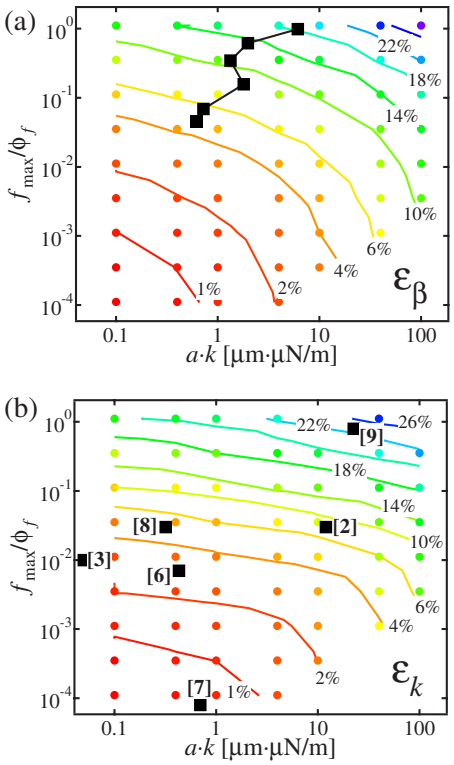

FIG. 7. (Color online) Contour plot of (a) ε_β and (b) ε_k interpolated from a grid of values (dots) for combinations of ak (bottom axis) and f_{max}/ϕ_f (left axis). ε_β for $f_{max}=100$ kHz from Fig. 6(a) is indicated by squares in (a). ε_k for the typical experiments employing optical trapping as listed in Table III is indicated by squares in (b).

of the error in percent obtained as a function of ak and f_{max}/ϕ_f. The x axis represents the product ak and the y axis represents the ratio f_{max}/ϕ_f. The lines are interpolated from a grid of calculated values (dots). In such representation, the error can be read from the figure directly for any combination of a, k, and f_{max}. The values of ε_β obtained from our data shown in Fig. 6(a) for $f_{max}=100$ kHz are represented by squares in Fig. 7(a). We see that the calibration error considerably increases with the sphere's radius, spring constant, and acquisition frequency.

Table III shows a selection of typical experiments using optical traps and gives an upper limit for the calibration error made when ignoring hydrodynamic memory effects. The sphere size, spring constant, and acquisition frequency are listed for each of the experiments. We take $f_{max}=f_{Nyq}=f_S/2$, and calculate ak and f_{max}/ϕ_f for each. Using Figs. 7(a) and 7(b), we estimate ε_β and ε_k, respectively.

Studies on molecular motors use small sphere sizes and low spring constants, and error in calibration is below 4%. Experimental tests of fluctuation theorems use larger spheres and errors may be above 20%. The error in the studies on diffusion can be reduced if the sphere size and spring constant are well chosen, as was done in Ref. [3]. However, all studies from Table III were made using sampling frequencies below 100 kHz. According to Fig. 7, extending the detection bandwidth to $f_S=500$ kHz leads to large calibration errors if

TABLE III. Possible calibration errors for selected experiments. In each experiment, data are acquired with an acquisition frequency f_S for a sphere of diameter a in a harmonic potential with spring constant k. For each, we calculate ak and f_{max}/ϕ_f (where $f_{max}=f_S/2$ corresponds to the Nyquist frequency), and estimate ε_β using Fig. 7(a) and ε_k using Fig. 7(b).

Reference	Research topic	a (μm)	k (μN/m)	f_S (kHz)	ak (μm μN/m)	f_{max}/ϕ_f	ε_β	ε_k
Pralle *et al.* [2]	Diffusion	0.5	24	40	12	0.03	<10%	<10%
Schäffer *et al.* [3]	Diffusion	0.26	0.2	66	0.05	0.01	<4%	<4%
Jeney *et al.* [6]	Molecular motors	0.22	2	50	0.43	0.007	<4%	<4%
Abbondanzieri *et al.* [7]	Molecular motors	0.35	2	0.2	0.7	0.00008	<1%	<1%
Wang *et al.* [8]	Fluctuation theorems	3.15	0.1	1	0.32	0.03	<4%	<6%
Trepagnier *et al.* [9]	Fluctuation theorems	5.03	4.5	10	22.6	0.79	<22%	<26%

memory effects are ignored. Then, accounting for the hydrodynamic memory effect becomes unavoidable.

V. CONCLUSIONS

In conclusion, we measured the motion of a single micrometer-sized sphere in an optical trap. We compare our data to the theory of Brownian particle in a harmonic potential that accounts for hydrodynamic memory effects, and find excellent agreement in the investigated time range of 2 μs to 1 ms and a frequency range of 1 to 250 kHz. When fitted to the data, both solutions give consistent values for the spring constant and the detector sensitivity.

Furthermore, we find that the motion of a particle is influenced by either memory effects or the trapping potential even for a sphere with a radius as small as 0.27 μm in a potential as weak as 1.5 μN/m. This excludes the existence of free diffusion and the linear increase of the mean-square displacement with time for the particle in optical trapping experiments.

We find that $5\phi_k$ is a convenient lower limit for the frequency range during which the particle can be considered as free from the influence of the trapping potential, where ϕ_k is the corner frequency of the power spectrum. This estimate is obtained by comparing data with the theory of the free Brownian particle that accounts for memory effects. A similar analysis is performed for the time domain. In particular, our experiment with a micrometer sized sphere in the softest trap gives the lower limit $5\phi_k \approx 300$ Hz. Therefore, under these conditions, the sphere probes only its local environment for approximately three decades in frequency (300 Hz–250 kHz).

Additionally, we find that neglecting memory effects leads to calibration errors that are higher than 10% when data are acquired with an acquisition frequency higher than 200 kHz for particles with radii above 0.5 μm. Hence, we suggest to check the presence of memory effects for each experiment, since calibration errors increase in a nontrivial fashion with particle size, spring constant, and acquisition frequency.

ACKNOWLEDGMENTS

We are grateful to J. Lekki for help in data acquisition, to T. Feher for help in fast data analysis, and to E. Bertseva, H. Flyvbjerg, C. Guzmán, and T. Piližota for discussions. B.L. acknowledges the financial support of the Swiss National Science Foundation and its NCCR "Nanoscale Science." We thank EPFL for funding the experimental equipment.

[1] A. Ashkin, J. M. Dziedzic, J. E. Bjorkholm, and S. Chu, Opt. Lett. **11**, 288 (1986).
[2] A. Pralle, E.-L. Florin, E. H. K. Stelzer, and J. K. H. Hörber, Appl. Phys. A: Mater. Sci. Process. **66**, S71 (1998).
[3] E. Schäffer, S. F. Nørrelykke, and J. Howard, Langmuir **23**, 3654 (2007).
[4] M. Atakhorrami, G. H. Koenderink, C. F. Schmidt, and F. C. MacKintosh, Phys. Rev. Lett. **95**, 208302 (2005).
[5] T. G. Mason, K. Ganesan, J. H. van Zanten, D. Wirtz, and S. C. Kuo, Phys. Rev. Lett. **79**, 3282 (1997).
[6] S. Jeney, E. H. K. Stelzer, H. Grubmüller, and E.-L. Florin, ChemPhysChem **5**, 1150 (2004).
[7] E. A. Abbondanzieri, W. J. Greenleaf, J. W. Shaevitz, R. Landick, and S. M. Block, Nature (London) **438**, 460 (2005).
[8] G. M. Wang, E. M. Sevick, E. Mittag, D. J. Searles, and D. J. Evans, Phys. Rev. Lett. **89**, 050601 (2002).
[9] E. H. Trepagnier, C. Jarzynski, F. Ritort, G. E. Crooks, C. J. Bustamante, and J. Liphardt, Proc. Natl. Acad. Sci. U.S.A. **42**, 15038 (2004).
[10] M. Atakhorrami, J. I. Sulkowska, K. M. Addas, G. H. Koenderink, J. X. Tang, A. J. Levine, F. C. MacKintosh, and C. F. Schmidt, Phys. Rev. E **73**, 061501 (2006).
[11] K. Berg-Sørensen, E. J. G. Peterman, L. Oddershede, M. van Dijk, E.-L. Florin, C. F. Schmidt, and H. Flyvbjerg, Proc. SPIE **5514**, 419 (2004).
[12] A. Rohrbach, C. Tischer, D. Neumayer, E.-L. Florin, and E. H. K. Stelzer, Rev. Sci. Instrum. **75**, 2197 (2004).
[13] V. Vladimirsky and Ya. Terletzky, Zh. Eksp. Teor. Fiz. **15**, 259 (1945). For English translation, see V. Lisy and J. Tohtova, e-print arXiv:cond-mat/0410222.

[14] E. J. Hinch, J. Fluid Mech. **72**, 499 (1975).
[15] D. A. Weitz, D. J. Pine, P. N. Pusey, and R. J. A. Tough, Phys. Rev. Lett. **63**, 1747 (1989).
[16] B. Lukić, S. Jeney, C. Tischer, A. J. Kulik, L. Forró, and E.-L. Florin, Phys. Rev. Lett. **95**, 160601 (2005).
[17] K. C. Neuman and S. M. Block, Rev. Sci. Instrum. **75**, 2787 (2004).
[18] K. Berg-Sørensen and H. Flyvbjerg, Rev. Sci. Instrum. **75**, 594 (2004).
[19] A. Rohrbach, Phys. Rev. Lett. **95**, 168102 (2005).
[20] H. J. H. Clercx and P. P. J. M. Schram, Phys. Rev. A **46**, 1942 (1992).
[21] F. Reif, *Fundamentals of Statistical and Thermal Physics* (McGraw-Hill, Singapore, 1985).
[22] As the particle's position $x(t)$ is a variable following a Gaussian distribution and $\langle \Delta x^2(t) \rangle$ corresponds to the second moment σ^2 of $x(t)$, the standard deviation of $X(t)$ is equal to $\sqrt{2}\sigma^2$. Since the standard deviation of $X(t)$ is larger than the expected value due to the diffusion process itself, it is not shown in Fig. 2(a). Furthermore, a weighted least-squares fitting cannot be performed for $X(t)$, and a statistical measure of goodness of fit for k and β can be obtained only for $\tilde{X}(f)$, as in Ref. [18].
[23] τ_M can be obtained by solving the equation $\partial X(t)/\partial t|_{\tau_M}=0$. Since it is a transcendental equation, an analytical solution for τ_M does not exist. Similarly, $\partial \tilde{X}(f)/\partial f|_{\phi_k}=0$ is also transcendental, and an analytical solution for ϕ_M does not exist either.